Journal of Materials Chemistry A

PAPER

View Article Online
View Journal | View Issue

Cite this: J. Mater. Chem. A, 2016, 4, 13899

Mesoporous graphitic carbon microtubes derived from fullerene C_{70} tubes as a high performance electrode material for advanced supercapacitors†

Partha Bairi,[a] Rekha Goswami Shrestha,[a] Jonathan P. Hill,[a] Toshiyuki Nishimura,[b] Katsuhiko Ariga*[a] and Lok Kumar Shrestha*[a]

Received 14th June 2016
Accepted 8th August 2016

DOI: 10.1039/c6ta04970b

www.rsc.org/MaterialsA

Direct conversion of mesoporous crystalline fullerene C_{70} microtubes into mesoporous graphitic carbon microtubes by heat treatment at high temperature (2000 °C) with retention of the initial one-dimensional tubular morphology is reported. The walls of the resulting graphitic carbon microtubes are composed of ordered conjugated sp^2 carbon with a robust mesoporous framework structure. Cyclic voltammetry and chronopotentiometry (charge–discharge) measurements revealed that this new carbon material exhibits high specific capacitance *ca.* 212.2 F g^{-1} at a scan rate of 5 mV s^{-1} and 184.6 F g^{-1} at current density 0.5 A g^{-1}. Furthermore, the material showed high rate performance. These results demonstrate that mesoporous graphitic carbon microtubes derived from the π-electron carbon source fullerene C_{70} can be a promising electrode material for application in high performance electrochemical supercapacitors.

Introduction

There is a burgeoning demand for sustainable high-performance energy-storage devices because of continuously increasing energy demands and the resulting environmental concerns.[1] Supercapacitors or electrochemical supercapacitors are some of the most convenient energy storage devices due to their high power capabilities, long lives, low maintenance and cost-per-cycle, low internal resistance and fast dynamic charge propagation.[2–6] Electrochemical supercapacitors have much greater power densities than traditional batteries and fuel cells, and also possess much larger energy densities than conventional dielectric capacitors.[2–6] Currently, supercapacitors are used in consumer electronics, memory backup systems, for industrial power and energy management, and recently they have been used in state-of-the-art aerospace applications in the Airbus A380.[7] However, the energy density of supercapacitors (1–10 W h kg^{-1}) remains low when compared with lead acid batteries (30–40 W h kg^{-1}), lithium ion batteries (160 W h kg^{-1}) and fuel cells.[8,9] To address this issue, special efforts have been made to improve the energy performance of supercapacitors through the introduction of new electrode materials, which might offer high specific capacitances '*C*',[2,7] and which can operate over a wide potential window '*V*'. These new materials would facilitate the assembly of effective energy storage systems since energy storage is proportional to CV^2.[8]

Mesoporous carbon materials are the leading electrode materials for commercial supercapacitors because of their outstanding cycle stability, wide voltage operating range (0–3 V) and low cost.[7,10–12] Therefore, the development of novel mesoporous carbon materials with high specific capacitances and energy densities would be advantageous. Extensive research has been carried out on the production of high quality carbon of uniform pore size distribution, large surface area and large pore volume.[13] These materials are generally prepared using a hard-templating approach[14–18] although direct self-assembly of amphiphilic molecules as a soft template has also been used as an alternative method.[19,20] Furthermore, for energy storage applications, nanoporous graphitic carbons having extended conjugated π-systems are advantageous.[21] Graphitization promotes the stability of the carbon matrix and concurrently enhances the electrical conductivity while reducing the internal resistance, which is important in determining the rate capabilities and power densities of the resulting materials.[22–25] Although mesoporous graphitic carbon has been prepared using block copolymers, phenolic resins, or small molecules as precursors,[26] the π-electron rich functional molecule fullerene C_{70} has not been explored as a carbon source for the production of high surface area graphitic nanoporous carbons.[21] Fullerene, which can be regarded as a zero dimensional functional molecule, can form higher dimensional nanostructures at liquid–liquid interfaces.[27–34] The resulting self-assembled fullerene

[a]World Premier International Center for Materials Nanoarchitectonics (WPI-MANA), National Institute for Materials Science (NIMS), 1-1 Namiki, Tsukuba 305-0044, Japan. E-mail: SHRESTHA.Lokkumar@nims.go.jp; ARIGA.Katsuhiko@nims.go.jp

[b]Sialon Unit, Environment and Energy Materials Division, National Institute for Materials Science (NIMS), 1-1 Namiki, Tsukuba 305-0044, Ibaraki, Japan

† Electronic supplementary information (ESI) available: Additional SEM, TEM, HR-TEM, FT-IR, TGA and CV data. See DOI: 10.1039/c6ta04970b

nanostructures can be directly converted into nanoporous carbon containing a graphitic microstructure but keeping the initial morphology. Due to their well-defined morphologies, these fullerene-derived graphitic structures, composed of extended conjugated sp^2 carbon with a robust mesoporous framework structure, are expected to display excellent supercapacitor performances.

In this contribution, we report the fabrication of mesoporous fullerene C_{70} microtubes (FT_15) with highly crystalline pore walls and their direct conversion into mesoporous graphitic carbon tubes with extended conjugated sp^2 carbon with a robust framework structure. FT_15 was produced using an ultrasonic liquid–liquid interfacial precipitation (ULLIP) method at 15 °C. FT_15 upon heat-treatment at high temperature (2000 °C) in vacuum yielded graphitic carbon with retention of the original tube morphology. This newly synthesized highly graphitic robust mesoporous carbon microtube (HTFT_2000) exhibited high specific capacitances *ca.* 212.2 F g^{-1} at a scan rate of 5 mV s^{-1} and 184.6 F g^{-1} at current density 0.5 A g^{-1}. Retention of specific capacitance value is observed at a high current density and scan rate that indicates the good rate performance of HTFT_2000. We believe that this novel carbon material is a suitable electrode material for advanced electrochemical supercapacitors.

Experimental section

Synthesis of mesoporous C_{70} microtubes

Mesoporous fullerene C_{70} tubes (FT_15) were synthesized by using an ultrasonic liquid–liquid interfacial precipitation (ULLIP) method (Scheme S1 in the ESI†). Fullerene C_{70} solution in 1,2-dichlorobenzene (DCB, 3.0 mg mL^{-1}) was prepared by dissolving pristine C_{70} powder (60 mg, 99%, MTR Ltd, USA) in 1,2-dichlorobenzene (20 mL) with ultrasonication for 30 min. In a typical crystallization, C_{70} solution (1 mL) was placed in a clean 13.5 mL glass bottle and stored in an incubator at 15 °C. After 30 min, 5 mL of isopropyl alcohol (IPA), which had also been stored at 15 °C, was slowly added to the C_{70} solution leading to a layered situation with a clear interface between the C_{70} solution and IPA. The resulting mixture was stored at 15 °C without mechanical disturbance for 1 h. Light agitation (hand shaking) was then applied followed by sonication for 30 s. The resulting mixture was again stored at 15 °C in an incubator for 48 h. Finally, FT_15 was washed several times with a large amount of IPA to completely remove DCB. Note that complete removal of DCB from FT_15 is absolutely necessary. The presence of even small quantities of DCB will solubilize FT_15 causing recrystallization to other products due to the high solubility of C_{70} in DCB (36.2 mg mL^{-1}). The resulting FT_15 was heat-treated at 900 °C at a temperature ramp of 2° min^{-1} under an argon atmosphere with the product of this procedure referred to as HTFT_900.

Production of mesoporous graphitic carbon tubes

For the production of mesoporous graphitic carbon tubes, FT_15 was heat treated at high temperature (2000 °C) in vacuum (7×10^{-3} Pa) using an FVHP-1-3, FTR-20-3VH (Fujidempa Kogyo Co., Ltd, Osaka, Japan). The product obtained in this procedure is referred to as HTFT_2000.

Characterization

Scanning electron microscopy (SEM) images of FT_15, HTFT_900 and HTFT_2000 were obtained by using a Hitachi Model S-4800 field effect scanning electron microscope (FE-SEM) operating at an accelerating voltage of 10 kV. SEM samples were prepared by dropping suspensions of microtubes in IPA on cleaned silicon wafers followed by drying at 80 °C. All microtube samples were coated with platinum (approx. 2 nm) using a Hitachi S-2030 ion coater. Transmission electron microscopy (TEM) images and selected area electron diffraction patterns (SAED) of the microtube samples were obtained using a transmission electron microscope (JEOL Model JEM-2100F operating at 200 kV). TEM samples were prepared by dropping suspensions of all microtubes in IPA onto standard carbon-coated copper grids. TEM samples were dried under reduced pressure at 80 °C for 24 h prior to TEM measurements. FT-IR spectra of pristine fullerene C_{70} and FT_15 were recorded using a Nicolet 4700 FT-IR instrument, Thermo Electron Corporation. Thermogravimetric analysis of FT_15 was performed using a SII Instrument (Model Exstar 600) under an argon gas atmosphere at a heating rate of 10 °C min^{-1}. Powder X-ray diffraction (pXRD) patterns of pristine C_{70} and the microtube samples were recorded at 25 °C on a Rigaku RINT2000 diffractometer with Cu-Kα radiation ($\lambda = 0.1541$ nm). Raman scattering spectra of the microtubes were recorded using a Jobin-Yvon T64000 Raman spectrometer. Raman samples were prepared on a clean silicon wafer and dried at 80 °C and excited using a green laser of wavelength 514.5 nm at 0.01 mW power. Nitrogen adsorption–desorption isotherms were recorded on an automatic adsorption instrument (Quantachrome Instruments, Autosorb-iQ2, USA) at liquid nitrogen temperature 77.35 K. For each measurement, about 20 mg of sample was degassed for 24 h at 100 °C prior to the measurements. X-ray photoelectron spectroscopy (XPS) of the microtubes and pristine C_{70} was performed on a Theta Probe spectrometer (Thermo Electron Co., Germany) using monochromated Al-Kα radiation (photon energy 15 keV, maximum energy resolution 0.47 eV). High resolution spectra for core level C 1s were recorded in 0.05 eV steps. A built-in electronic charge neutralizing electron flood gun was used to prevent sample charging.

Cyclic voltammetry (CV)

Electrochemical performances of pristine C_{70} and the microtube samples were studied by cyclic voltammetry (CV) and charge–discharge experiments with a three-electrode system in 1 M aqueous H_2SO_4 solution at 25 °C. Prior to CV and charge–discharge experiments, we modified glassy carbon electrodes with the respective sample. Each sample (1 mg) was placed in a 5 mL vial and water–ethanol mixture (4 : 1 v/v, 1 mL) was added followed by sonication of the mixture for about 30 min until complete dispersion had occurred. For modification of the GC electrode, the microtube dispersion (5 μL) was dropcast onto

a cleaned glassy carbon electrode followed by drying in an oven for 1 h at 60 °C. Then Nafion solution in ethanol (0.5% w/v, 5 μL) was dropped on the dry microtube-modified electrode. Finally, the microtube-modified electrode was dried at 60 °C for 12 h. All measurements were carried out using an ALS/CH Model 850D Electrochemical Analyzer in the potential range from 0 to 0.8 V (*vs.* Ag/AgCl).

Calculations

The electrochemical performance of the modified electrodes in H_2SO_4 (1 M) was examined by cyclic voltammetry (CV) and galvanostatic charge–discharge experiments. The capacitance (C_s) was calculated from the galvanostatic discharge process according to the following equation:

$$C_s = \frac{I \times t}{m \times \Delta V} \quad (1)$$

where I is the discharge current (A), t is the discharge time (s), ΔV is the voltage change (V) during the discharge process and m is the total mass of the active electrode material (g).

The electrochemical performances of the modified electrodes were examined by CV. The capacitance of the electrode was calculated according to the following equation:

$$C_s = \frac{\int I \mathrm{d}V}{mS\Delta V} \quad (2)$$

where I is the current (A), S is the scan rate (mV s^{-1}), ΔV is the absolute value of the potential window (V), and m is the total mass of the active electrode material (g).

I–V measurements

Microtubes were dispersed in isopropanol (1 mg mL^{-1}), drop-cast on a cleaned silicon dioxide substrate and dried at 60 °C. Four-terminal electrical measurement was realized on a microscopic structure in air, using a home-built quadruple-scanning-probe microscope (QSPFM). The QSPFM has four probes whose positions are individually controlled by obtaining images of a sample in the manner of atomic force microscopy (AFM), and uses the probe as contacting electrodes for electrical measurements. A specially arranged tuning fork probe (TFP) is used as a self-detection force sensor to operate each probe in a frequency modulation AFM mode, resulting in simultaneous imaging of the same microscopic feature on an insulator using the four TFPs. Four-terminal electrical measurement is then demonstrated in air by placing each probe electrode in contact with the sample on a silicon dioxide film. The detailed theory and methodology can be found elsewhere.[35]

Results and discussion

Fullerene C_{70} microtubes (FT_15) were produced at the interface between isopropyl alcohol (IPA) and a solution of C_{70} in 1,2-dichlorobenzene (DCB) at 15 °C as described in the experimental section. FT_15 was used as a π-electron carbon source for the production of high surface area mesoporous carbon and mesoporous graphitic carbon with crystalline pore walls. FT_15 was heat-treated at 900 °C under an argon atmosphere (HTFT_900). FT_15 was also heat-treated at a higher temperature (2000 °C in vacuum) to obtain mesoporous graphitic carbon microtubes (HTFT_2000).

Fig. S1† shows typical SEM images of fullerene C_{70} microtubes (FT_15) obtained by using the ULLIP method.[27] The narrow diameter distribution (Fig. S2†) of FT_15 is an indication of homogeneous crystal growth. The average diameter of FT_15 is *ca.* 850 ± 31 nm. Transmission electron microscopy (TEM) images (Fig. S3†) clearly demonstrate a tubular morphology with a well-developed mesoporous structure. The highly crystalline pore walls or framework structure of FT_15 can be observed in high resolution TEM (HR-TEM) images (Fig. S4†). Coherently extended lattice fringes of fullerene C_{70} over some nanopores with a spot type selected area electron diffraction (SAED) pattern (inset; Fig. S4c†) confirm the high degree of crystallinity of the pore walls. The solvated solid structure of FT_15 was confirmed by FT-IR and thermogravimetric analyses (TGA) (Fig. S5 and S6†). Tube formation in the DCB–IPA system is considered to occur by a well-known core dissolution mechanism.[36,37] Initially, fullerene C_{70} solvated microrods are formed in which the surfaces of the solvated microrods are insoluble in the mixed solvent. Over time, the less stable core of the solvated microrod re-dissolves in the good solvent (DCB) forming the tubular structure. The core dissolution mechanism is supported by TEM analysis (Fig. S7†). We found that some of the microtubes were incompletely formed and some irregular structures at the inner walls of the microtubes were also observed. These observations indicate that the core dissolution is not very uniform.

SEM images of HTFT_900 (Fig. S8†) indicate retention of the tubular morphology of the starting fullerene C_{70} microtubes after carbonization at 900 °C. High resolution SEM images (Fig. S8†) of HTFT_900 demonstrate that the walls of the microtubes become highly porous compared to FT_15. TEM images (Fig. S9†) also revealed a highly porous tubular structure. A careful observation of HR-TEM images (Fig. S10†) reveals the existence of partial lattice fringes of C_{70} demonstrating that heat-treatment of FT_15 at 900 °C did not completely convert the fullerene C_{70} crystal into amorphous carbon with some C_{70} crystal remaining in the system (further confirmed by the SAED pattern (inset; Fig. S10c†)). This signifies the strong bonding forces between C_{70} molecules along the tube growth axis. Note that heat-treatment of fullerene C_{60} crystals at 900 °C causes a complete conversion of fullerene C_{60} into amorphous carbon.[38] Fullerene C_{70} has lower strain and possesses greater thermal stability than fullerene C_{60}.

Heat-treatment of FT_15 at 2000 °C did not alter the 1D tubular morphology of the original crystals (Fig. 1a and b and S11†). Furthermore, additional mesopores are developed on the tube surface. The random distribution of these mesopores can be observed in the TEM images of HTFT_2000 (Fig. 1c and S12†) with HR-TEM images (Fig. 1d and S13†) confirming that crystalline C_{70} is completely transformed into highly graphitic carbon.

The well-developed mesoporous structure of the heat-treated samples (HTFT_900 and HTFT_2000) leads to observation of

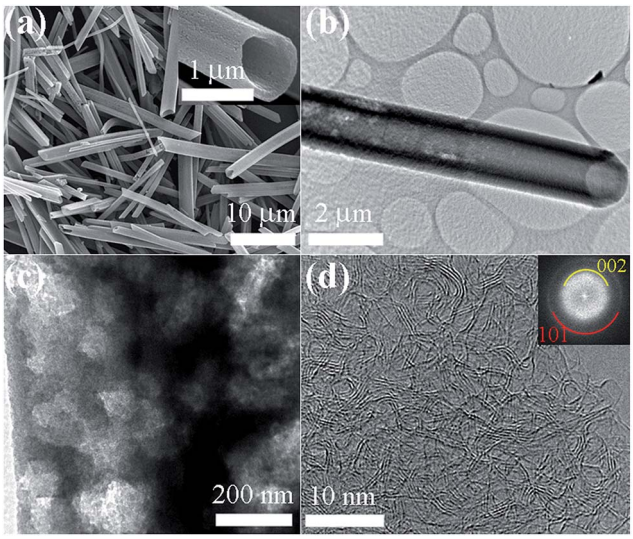

Fig. 1 (a) FE-SEM images of HTFT_2000, (b) TEM image of HTFT_2000 showing the tubular structure, and (c and d) HR-TEM images of a single microtube HTFT_2000 (inset of panel (d): SAED pattern).

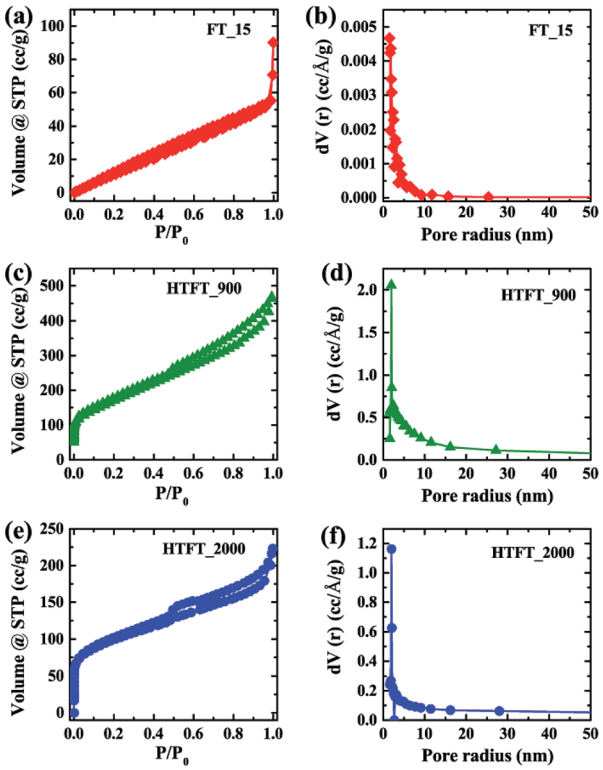

Fig. 2 (a and b), (c and d) and (e and f) Nitrogen adsorption–desorption isotherm and plot of pore radius *vs.* d*V*(*r*) of FT_15, HTFT_900 and HTFT_2000, respectively.

type IV behaviour of their nitrogen adsorption–desorption isotherms (Fig. 2c and e) with hysteresis loops demonstrating a cage-like structure. The isotherm of FT_15 reveals that it does not exhibit saturation at higher pressures due to the formation of large size pores (Fig. 2a). The pore size distribution curves indicate the existence of mesoporous structures with average pore sizes *ca.* 3.08 nm (FT_15), 3.88 nm (HTFT_900), and 3.88 nm (HTFT_2000). Thermal treatment caused increased porosity with the result that surface areas of heat-treated samples were also increased. The Brunauer–Emmett–Teller (BET) surface areas of HTFT_900 and HTFT_2000 are respectively estimated to be 609 and 334 $m^2 g^{-1}$, both much greater than that of FT_15 prior to heat treatment (85.6 $m^2 g^{-1}$). Note that the obtained BET specific surface areas of HTFT_900 and HTFT_2000 are relatively lower than those of activated carbons due to the lack of a microporous structure.[39] Most of the activated carbons contain a microporous structure which is responsible for the high surface area. The lower surface area of HTFT_2000 can be attributed to the graphitization and a denser carboniferous structure (Fig. S13†).

The crystal structures of FT_15 prior to and following heat treatment were studied and compared with those of the pristine C_{70} powder. The XRD pattern of pristine C_{70} (Fig. 3a) can be indexed as a hexagonal close packed (hcp) structure[40] with lattice parameters $a = 1.08$ and $c = 1.74$ nm, whereas the XRD pattern of FT_15 was indexed as a face-centered cubic (fcc) structure (Fig. 3a) with cell dimension $a = 1.49$ nm.[41] XRD peaks corresponding to (111) and (222) planes of the fcc structure remain in HTFT_900. After graphitization at 2000 °C, XRD peaks corresponding to crystalline C_{70} are absent and a new diffraction peak corresponding to the (002) plane of graphitic carbon appeared at 26.02° (d = 0.342 nm).[21] Furthermore, a broad diffraction peak appearing at approximately 43.5° corresponds to the (101) graphite plane and confirms the presence of weak intralayer-ordering of the graphene layers in HTFT_2000.

Thermal decomposition of highly crystalline fullerene C_{70} crystals into amorphous and graphitic carbon was further confirmed by Raman scattering. The Raman spectrum of FT_15 (Fig. 3b) is very similar to that of pristine C_{70}, indicating that the impact of solvent molecules on C_{70} in the crystal is negligible and that their rotation is still free in the solvated crystal.[42] Raman bands corresponding to crystalline C_{70} disappeared in heat-treated samples and new bands corresponding to D and G bands of carbon emerge at *ca.* 1340 and 1582 cm^{-1}.[43] In the HTFT_2000 sample, an additional Raman band at 2678 cm^{-1} (2D band) also appeared, which indicates the formation of highly crystalline carbon materials. The D band (defect-induced) corresponds to the presence of disorder in the sp^2 carbon system whereas the G band represents a graphitic structure corresponding to the stretching vibration of the C–C bond in graphitic materials and is common to all sp^2 carbon systems.

X-ray photoelectron spectroscopy (XPS) was employed to characterize the chemical states of elements on the surface of the tubes before and after heat-treatment. As can be seen in the XPS survey spectrum (Fig. 3c) pristine C_{70} clearly displays core level peaks for carbon (C 1s) and oxygen (O 1s) (since the surface of pristine C_{70} is oxidized). The relative intensity of the O 1s spectrum is smaller in FT_15 and the heat-treated samples (HTFT_900 and HTFT_2000) than in pristine C_{70}. The deconvoluted XPS C 1s core level peaks of all the samples (pristine C_{70},

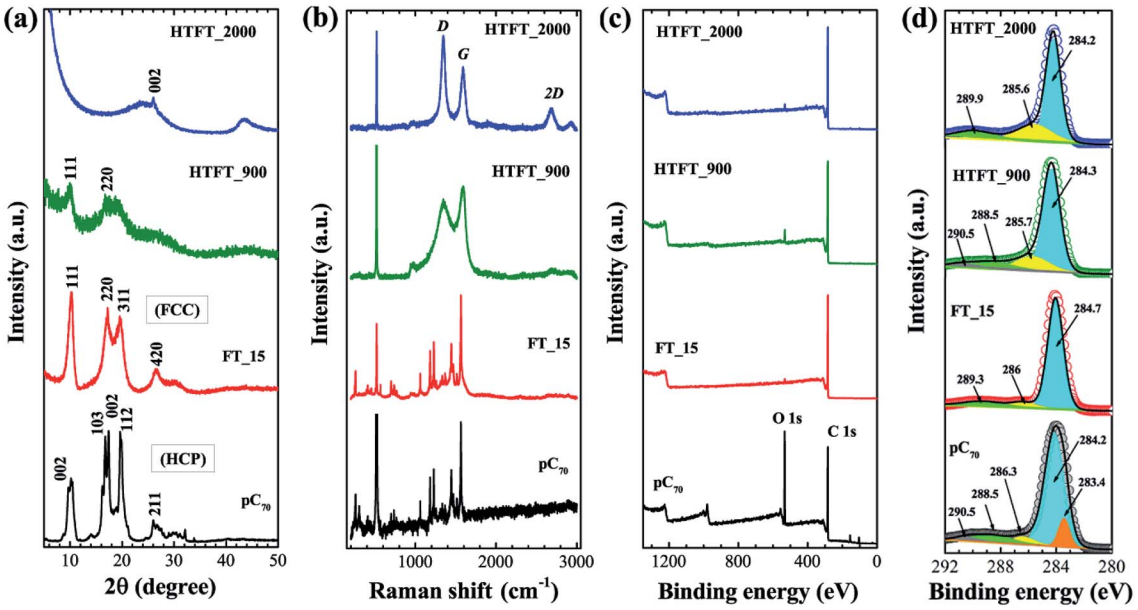

Fig. 3 (a) and (b) Powder XRD pattern and Raman scattering of pristine C_{70}, FT_15, HTFT_900 and HTFT_2000, (c) and (d) survey XPS spectra and C 1s core level XPS spectra with peak fit of pristine C_{70}, FT_15, HTFT_900 and HTFT_2000, respectively.

FT_15, HTFT_900 and HTFT_2000) indicate the presence of C–C (sp^3), C=C (sp^2), and C=O (Fig. 3d).

Electrochemical supercapacitive properties of FT_15 before and after heat-treatment are presented in Fig. 4. Cyclic voltammetry (CV) curves were recorded in 1 M aqueous H_2SO_4 electrolyte within the potential range 0 to 0.8 V (*vs.* Ag/AgCl) using a three electrode system. The CV curves of HTFT_2000 (Fig. 4a) show very rapid current response and exhibit a quasi-rectangular shape at low scan rates, features that are similar to electrical double layer capacitors (EDLCs).[44,45] At higher scan rates the CV profile departs from an ideal rectangular shape due to the presence of oxygen containing surface functional groups or other electrochemically unstable species and also due to the obstruction of diffusion of the electrolyte ions in the mesoporous walls of the microtubes. Note that, despite a high surface area (609 $m^2\ g^{-1}$), the current density of HTFT_900 is comparable to that of FT_15 (Fig. 4b) demonstrating that carbonization of FT_15 at 900 °C does not improve the electrochemical supercapacitive properties. This is probably due to the low conductivity of the material caused by its high content of amorphous carbon. Conversely, HTFT_2000 displayed very high current density compared to FT_15 and FT_900 due to the graphitic structure of its crystalline pore walls. The specific capacitance of HTFT_2000 is *ca.* 212.5 F g^{-1} at a scan rate of 5 mV s^{-1}. Specific capacitances of FT_15 and HTFT_900 were *ca.* 21.7 and 26.4 F g^{-1}, respectively (Fig. 4c and S14†). Note that due to the hollow tubular structure, mesoporous graphitic pore walls and high conductivity, HTFT_2000 sustains high capacitance even at higher scan rates. About 49 and 35% capacitance retention is observed at high scan rates of 100 and 300 mV s^{-1}, respectively.

Galvanostatic charge–discharge measurements were also carried out at different current densities in a three-electrode system to obtain further insight into the electrochemical performance of FT_15, HTFT_900 and HTFT_2000 electrodes (Fig. 4b and S15†). The observed triangular shaped charge–discharge (CD) curves (Fig. 4d) indicate that HTFT_2000 could be used as an electrode material for EDLCs. From the CD curves, the specific capacitances of HTFT_2000 are *ca.* 184.6 and 165.5 F g^{-1} at current densities of 0.5 and 1 A g^{-1}, respectively. About 53 and 37% capacitance retention was observed at high current densities of 5 and 10 A g^{-1}, respectively (Fig. 4d and e), demonstrating the good rate performance of HTFT_2000.[46] Long-term cyclic stability of an electrode is essential for supercapacitor applications. Here, we have studied the cyclic stability of the HTFT_2000 electrode by recording CD curves over 1000 cycles at a current density of 10 A g^{-1}. Despite the high rate performance, the cyclic stability of HTFT_2000 is not so good. Capacitance retention of about 78% is observed after 1000 cycles (Fig. 4f). Minute observation reveals that the capacitance of HTFT_2000 drops rapidly with cycling at the beginning stage and then drops slowly with further increasing the cycle number. About 17.5% capacitance drops after 100 cycles and after that only 4.5% drops even after 1000 cycles. A sudden drop of the capacitance value of HTFT_2000 at the initial stage is caused due to the presence of oxygenated functional groups on the surface of HTFT_2000.

Overall, our novel mesoporous graphitic carbon tubes exhibit excellent electrochemical performance including large capacitance in excess of those reported for pure graphene,[47–49] conventional mesoporous carbon,[50,51] nitrogen and boron doped graphene,[52] nitrogen-doped carbon and graphene aerogel,[53–59] and resol-derived carbon/graphene aerogel composites.[60–62] The excellent electrochemical supercapacitive properties of HTFT_2000 can be attributed to the high surface area of the conductive graphitic carbon tubes.[63] Graphitization

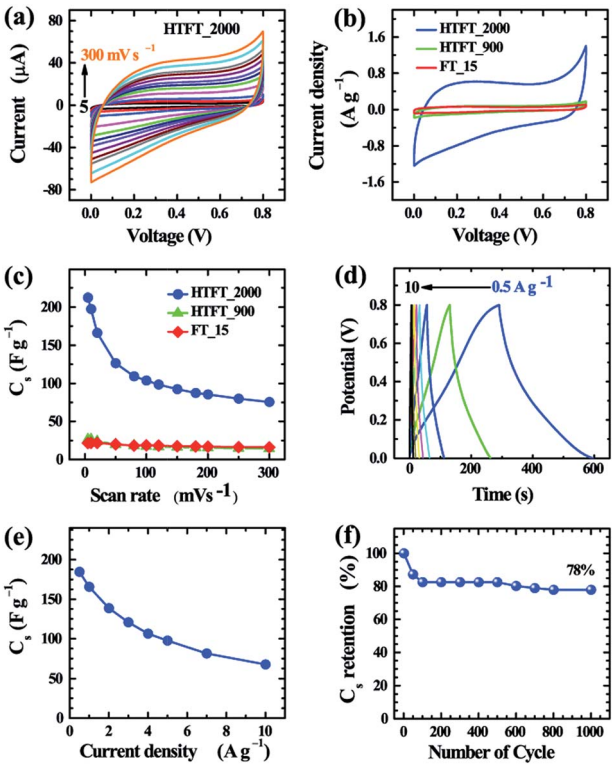

Fig. 4 (a) CV curves of graphitized carbon microtubes HTFT_2000 with different scan rates (5 to 300 mV s^{-1}), (b) Comparison of the current densities of all microtube samples from CV curves, (c) Specific capacitances obtained from CV curves of the microtube samples at different scan rates, (d) Charge–discharge curves for HTFT_2000 at different current densities, (e) specific capacitance obtained from charge–discharge curves at different current densities, and (f) cyclic stability of the HTFT_2000 modified electrode from the charge–discharge experiment.

enhances the electrical conductivity (Fig. S16†) leading to a reduction in internal resistance, which contributes to enhancing the rate capability of HTFT_2000. Moreover, the 1D tubular morphology containing mesopores also improves charge transport in the supercapacitor electrode.[64,65] Thus, the highly graphitic mesoporous and 1D tubular morphology makes HTFT_2000 suitable as an electrode material for electrochemical supercapacitors.

Conclusions

We have fabricated mesoporous crystalline fullerene C_{70} tubes (FT_15) at a liquid–liquid interface and successfully converted them into highly robust graphitic carbons by heat-treatment at 2000 °C (HTFT_2000). The heat-treated sample HTFT_2000 retains the starting 1D tubular morphology and exhibits excellent electrochemical performance giving high specific capacitances of *ca.* 212.2 F g^{-1} at a scan rate of 5 mV s^{-1} and 184.6 F g^{-1} at a current density of 0.5 A g^{-1}. Furthermore, HTFT_2000 showed good rate capability required for supercapacitor device fabrication. Heat-treatment of FT_15 at 900 °C (HTFT_900) yielded mesoporous carbon with amorphous walls containing some undecomposed fullerene C_{70}. The specific capacitance of HTFT_900 was low (26.4 F g^{-1}) due to the lack of a graphitic structure, although the BET surface area was high (609 m^2 g^{-1}) compared to HTFT_2000 (334 m^2 g^{-1}). This highlights the importance of the conjugated graphitic framework structure of mesoporous carbons in the improvement of the overall electrochemical supercapacitor performance of these materials. We believe that these novel mesoporous graphitic carbon microtubes will open a new avenue in the porous carbon nanomaterials field due to their potential application as electrode materials in high performance supercapacitors.

Acknowledgements

This work was partially supported by World Premier International Research Center Initiative (WPI Initiative), MEXT, Japan.

Notes and references

1 J. R. Miller and P. Simon, *Science*, 2008, **321**, 651–652.
2 P. Simon and Y. Gogotsi, *Nat. Mater.*, 2008, **7**, 845–854.
3 G. Wang, L. Zhang and J. Zhang, *Chem. Soc. Rev.*, 2012, **41**, 797–828.
4 S.-M. Chen, R. Ramachandran, V. Mani and R. Saraswathi, *Int. J. Electrochem. Sci.*, 2014, **9**, 4072–4085.
5 N. Devillers, S. Jemei, M.-C. Pera, D. Bienaime and F. Gustin, *J. Power Sources*, 2014, **246**, 596–608.
6 J. R. Miller and A. F. Burke, *Electrochem. Soc. Interface*, 2008, **17**, 53–57.
7 (*a*) L. L. Zhang and X. S. Zhao, *Chem. Soc. Rev.*, 2009, **38**, 2520–2531; (*b*) D. Chen, Q. Wang, R. Wang and G. Shen, *J. Mater. Chem. A*, 2015, **3**, 10158–10173; (*c*) K. Chen and D. Xue, *J. Mater. Chem. A*, 2016, **4**, 7522–7537; (*d*) Y. Deng, Y. Xie, K. Zoua and X. Ji, *J. Mater. Chem. A*, 2016, **4**, 1144–1173.
8 A. Burke, *Electrochim. Acta*, 2007, **53**, 1083–1091.
9 R. R. Salunkhe, J. Lin, V. Malgras, S. X. Dou, J. H. Kim and Y. Yamauchi, *Nano Energy*, 2015, **11**, 211–218.
10 T. Chen and L. Dai, *J. Mater. Chem. A*, 2014, **2**, 10756–10775.
11 M. F. El-Kady, V. Strong, S. Dubin and R. B. Kaner, *Science*, 2012, **335**, 1326–1330.
12 J. Chmiola, G. Yushin, Y. Gogotsi, C. Portet, P. Simon and P. L. Taberna, *Science*, 2006, **313**, 1760–1763.
13 (*a*) C. Liang, Z. Li and S. Dai, *Angew. Chem., Int. Ed.*, 2008, **47**, 3696–3717; (*b*) R. K. Joshi, S. Alwarappan, M. Yoshimura, V. Sahajwalla and Y. Nishina, *Appl. Mater. Today*, 2015, **1**, 1–12.
14 J. Lee, S. Yoon, T. Hyeon, S. M. Oh and K. B. Kim, *Chem. Commun.*, 1999, 2177–2178.
15 S. Han, K. Sohn and T. Hyeon, *Chem. Mater.*, 2000, **12**, 3337–3341.
16 T. Kyotani, T. Nagai, S. Inoue and A. Tomita, *Chem. Mater.*, 1997, **9**, 609–615.
17 Z. X. Ma, T. Kyotani and A. Tomita, *Chem. Commun.*, 2000, 2365–2366.
18 Z. J. Li and S. Dai, *Chem. Mater.*, 2005, **17**, 1717–1721.

19 T. Kowalewski, N. V. Tsarevsky and K. Matyjaszewski, *J. Am. Chem. Soc.*, 2002, **124**, 10632–10633.
20 C. Liang and S. Dai, *J. Am. Chem. Soc.*, 2006, **128**, 5316–5317.
21 L. K. Shrestha, R. G. Shrestha, Y. Yamauchi, J. P. Hill, T. Nishimura, K. Miyazawa, T. Kawai, S. Okada, K. Wakabayashi and K. Ariga, *Angew. Chem., Int. Ed.*, 2015, **54**, 951–955.
22 Y. W. Zhu, S. T. Murali, M. D. Stoller, K. J. Ganesh, W. W. Cai, P. J. Ferreira, A. Pirkle, R. M. Wallace, K. A. Cychosz, M. Thommes, D. Su, E. A. Stach and R. S. Ruoff, *Science*, 2011, **332**, 1537–1541.
23 J. Tang, R. R. Salunkhe, J. Liu, N. L. Torad, M. Imura, S. Furukawa and Y. Yamauchi, *J. Am. Chem. Soc.*, 2015, **137**, 1572–1580.
24 L. Sun, C. Tian, Y. Fu, Y. Yang, J. Yin, L. Wang and H. Fu, *Chem.–Eur. J.*, 2014, **20**, 564–574.
25 M. Zhi, C. Xiang, J. Li, M. Li and N. Wu, *Nanoscale*, 2013, **5**, 72–88.
26 (*a*) D. W. Wang, F. Li, M. Liu, G. Q. Lu and H. M. Cheng, *Angew. Chem., Int. Ed.*, 2008, **47**, 373–376; (*b*) B. Senthilkumar, Z. Khan, S. Park, K. Kim, H. Ko and Y. Kim, *J. Mater. Chem. A*, 2015, **3**, 21553–21561; (*c*) P. Su, L. Jiang, J. Zhao, J. Yan, C. Li and Q. Yang, *Chem. Commun.*, 2012, **48**, 8769–8771; (*d*) Z. C. Yang, C. H. Tang, Y. Zhang, H. Gong, X. Li and J. Wang, *Sci. Rep.*, 2013, **3**, 2925; (*e*) S. Jin, J. P. Hill, Q. Ji, L. K. Shrestha and K. Ariga, *J. Mater. Chem. A*, 2016, **4**, 5737–5744.
27 L. K. Shrestha, Q. Ji, T. Mori, K. Miyazawa, Y. Yamauchi, J. P. Hill and K. Ariga, *Chem.–Asian J.*, 2013, **8**, 1662–1679.
28 S. I. Cha, K. Miyazawa and J. D. Kim, *Chem. Mater.*, 2008, **20**, 1667–1699.
29 A. L. Briseno, S. C. B. M. Mannsfeld, M. Ling, S. Liu, R. J. Tseng, C. Reese, M. E. Roberts, Y. Yang, F. Wudl and Z. Bao, *Nature*, 2006, **444**, 913–917.
30 M. Sathish, K. Miyazawa, J. P. Hill and K. Ariga, *J. Am. Chem. Soc.*, 2009, **131**, 6372–6373.
31 (*a*) J. Kim, C. Park and H. C. Choi, *Chem. Mater.*, 2015, **27**, 2408–2413; (*b*) P. Bairi, K. Minami, W. Nakanishi, J. P. Hill, K. Ariga and L. K. Shrestha, *ACS Nano*, 2016, **10**, 6631–6637.
32 H. S. Shin, S. M. Yoon, Q. Tang, B. Chon, T. Joo and H. C. Choi, *Angew. Chem., Int. Ed.*, 2008, **47**, 693–696.
33 L. K. Shrestha, Y. Yamauchi, J. P. Hill, K. Miyazawa and K. Ariga, *J. Am. Chem. Soc.*, 2013, **135**, 586–589.
34 M. Sathish, K. Miyazawa and T. Sasaki, *Chem. Mater.*, 2007, **19**, 2398–2400.
35 (*a*) T. Nakayama, O. Kubo, Y. Shigaya, S. Higuchi, T. Hasegawa, C.-H. Jiang, T. Okuda, Y. Kuwahara, K. Takami and M. Aono, *Adv. Mater.*, 2012, **24**, 1675–1692; (*b*) S. Higuchi, O. Kubo, M. Aono and T. Nakayama, *Nanotechnology*, 2011, **22**, 285205–285211.
36 K. Miyazawa, *Sci. Technol. Adv. Mater.*, 2015, **16**, 13502–13512.
37 K. Miyazawa and J. Minato, *J. Mater. Res.*, 2005, **20**, 688–695.
38 R. Kato, K. Miyazawa, T. Nishimura and Z. M. Wang, *J. Phys.: Conf. Ser.*, 2009, **159**, 12024–12029.
39 (*a*) O. Ioannidou and A. Zabaniotou, *Renewable Sustainable Energy Rev.*, 2007, **11**, 1966–2005; (*b*) K. Yang, J. Peng, C. Srinivasakannan, L. Zhang, H. Xia and X. Duan, *Bioresour. Technol.*, 2010, **101**, 6163–6169; (*c*) S. Zhang, M. Zheng, Z. Lin, N. Li, Y. Liu, B. Zho, H. Pang, J. Cao, P. He and Y. Shi, *J. Mater. Chem. A*, 2014, **2**, 15889–15896.
40 M. Premila, C. S. Sundar, P. C. Sahu, A. Bharathi, Y. Hariharan, D. V. S. Muthu and A. K. Sood, *Solid State Commun.*, 1997, **104**, 237–242.
41 D. Liu, M. Yao, L. Wang, Q. Li, W. Cui, B. Liu, R. Liu, B. Zou, T. Cui, B. Liu, J. Liu, B. Sundqvist and T. Wagberg, *J. Phys. Chem. C*, 2011, **115**, 8918–8922.
42 V. Schettino, M. Pagliai and G. Cardini, *J. Phys. Chem. A*, 2002, **106**, 1815–1823.
43 M. A. Pimenta, G. Dresselhaus, M. S. Dresselhaus, L. G. Cancado, A. Jorioa and R. Saito, *Phys. Chem. Chem. Phys.*, 2007, **9**, 1276–1291.
44 (*a*) M. Pumera, *Electrochem. Commun.*, 2013, **36**, 14–18; (*b*) A. Ambrosi, C. K. Chua, A. Bonanni and M. Pumera, *Chem. Rev.*, 2014, **114**, 7150–7188; (*c*) R. Liu, L. Wan, S. Liu, L. Pan, D. Wu and D. Zhao, *Adv. Funct. Mater.*, 2015, **25**, 526–533.
45 R. Rajendran, L. K. Shrestha, K. Minami, M. Subramanian, R. Jayavelb and K. Ariga, *J. Mater. Chem. A*, 2014, **2**, 18480–18487.
46 (*a*) X. Wang, C. Yan, A. Sumboja, J. Yan and P. S. Lee, *Adv. Energy Mater.*, 2014, **4**, 1301240; (*b*) X. Wei, X. Jiang, J. Wei and S. Gao, *Chem. Mater.*, 2016, **28**, 445–458; (*c*) Q. Wang, J. Yan, Y. Wang, T. Wei, M. Zhang, X. Jing and Z. Fan, *Carbon*, 2014, **67**, 119–127; (*d*) W. Wei, X. Cui, W. Chen and D. G. Ivey, *J. Phys. Chem. C*, 2008, **112**, 15075–15083.
47 Z.-S. Wu, Y. Sun, Y.-Z. Tan, S. Yang, X. Feng and K. Muellen, *J. Am. Chem. Soc.*, 2012, **134**, 19532–19535.
48 Y. Xu, K. Sheng, C. Li and G. Shi, *ACS Nano*, 2010, **4**, 4324–4330.
49 M. D. Stoller, S. Park, Y. Zhu, J. An and R. S. Ruoff, *Nano Lett.*, 2008, **8**, 3498–3502.
50 H. Lu, W. Dai, M. Zheng, N. Li, G. Ji and J. Cao, *J. Power Sources*, 2012, **209**, 243–250.
51 D. Qu and H. Shi, *J. Power Sources*, 1998, **74**, 99–107.
52 A. Ambrosi, H. L. Poh, L. Wang, Z. Sofer and M. Pumera, *ChemSusChem*, 2014, **7**, 1102–1106.
53 L. F. Chen, X. D. Zhang, H.-W. Liang, M. Kong, Q.-F. Guan, P. Chen, Z.-Y. Wu and S.-H. Yu, *ACS Nano*, 2012, **6**, 7092–7102.
54 D. Hulicova-Jurcakova, M. Kodama, S. Shiraishi, H. Hatori, Z. H. Zhu and G. Q. Lu, *Adv. Funct. Mater.*, 2009, **19**, 1800–1809.
55 G. Lota, K. Lota and E. Frackowiak, *Electrochem. Commun.*, 2007, **9**, 1828–1832.
56 E. Frackowiak, G. Lota, J. Machnikowski, C. Vix-Guterl and F. Beguin, *Electrochim. Acta*, 2006, **51**, 2209–2214.
57 Y. J. Kim, Y. Abe, T. Yanagiura, K. C. Park, M. Shimizu, T. Iwazaki, S. Nakagawa, M. Endo and M. S. Dresselhaus, *Carbon*, 2007, **45**, 2116–2125.
58 F. Beguin, K. Szostak, G. Lota and E. A. Frackowiak, *Adv. Mater.*, 2005, **17**, 2380–2388.
59 Z.-S. Wu, A. Winter, L. Chen, Y. Sun, A. Turchanin, X. Feng and K. Müllen, *Adv. Mater.*, 2012, **24**, 5130–5135.

60 F. Meng, X. Zhang, B. Xu, S. Yue, H. Guo and Y. Luo, *J. Mater. Chem.*, 2011, **21**, 18537–18539.
61 Z. Wang, L. Yue, Z.-T. Liu, Z.-H. Liu and Z. Hao, *J. Mater. Chem.*, 2012, **22**, 14101–14107.
62 Y. Qian, I. M. Ismail and A. Stein, *Carbon*, 2014, **68**, 221–231.
63 Y. Li, G. Wangn, T. Wei, Z. Fann and Q. P. Yan, *Nano Energy*, 2016, **19**, 165–175.
64 M. Zhi, C. Xiang, J. Li, M. Li and N. Wu, *Nanoscale*, 2013, **5**, 72–88.
65 Z. Yu, L. Tetard, L. Zhai and J. Thomas, *Energy Environ. Sci.*, 2015, **8**, 702–730.